Foreshock and Aftershocks in Simple Earthquake Models

J. Kazemian, K. F. Tiampo, W. Klein, and R. Dominguez

Phys. Rev. Lett. **114**, 088501 — Published 25 February 2015

DOI: 10.1103/PhysRevLett.114.088501

Foreshock and aftershocks in simple earthquake models

J. Kazemian[1], K.F. Tiampo[1], W. Klein[2] and R. Dominguez[3]

[1]{Department of Earth Sciences, Western University, London, Ontario N6A 5B7, Canada}

[2]{Department of Physics and Center for Computational Sciences, Boston University, Boston, Massachusetts 02215, USA}

[3]{Department of Physics, Randolph-Macon College, Ashland, Virginia 23005, USA}

Correspondence to: J. Kazemian (jkazemia@alumni.uwo.ca)

Abstract

Many models of earthquake faults have been introduced that connect Gutenberg-Richter (GR) scaling to triggering processes. However, natural earthquake fault systems are composed of a variety of different geometries and materials and the associated heterogeneity in physical properties can cause a variety of spatial and temporal behaviors. This raises the question of how the triggering process and the structure interact to produce the observed phenomena. Here we present a simple earthquake fault model based on the Olami-Feder-Christensen (OFC) and Rundle-Jackson-Brown (RJB) cellular automata models with long-range interactions that incorporates a fixed percentage of stronger sites, or 'asperity cells', into the lattice. These asperity cells are significantly stronger than the surrounding lattice sites but eventually rupture when the applied stress reaches their higher threshold stress. The introduction of these spatial heterogeneities results in temporal clustering in the model that mimics that seen in natural fault systems along with GR scaling. In addition, we observe sequences of activity that start with a gradually accelerating number of larger events (foreshocks) prior to a mainshock that is followed by a tail of decreasing activity (aftershocks). This work provides further evidence that the spatial and temporal patterns observed in natural seismicity are strongly influenced by the underlying physical properties and are not solely the result of a simple cascade mechanism.

Understanding the dynamics of seismic activity is fundamental to investigation of the earthquake process. Simple models of statistical fracture have been used to test many of the typical assumptions and effective parameters inherent in the complicated dynamics of the earthquake fault system and their relative variability [1-9]. Most of these models assume a spatially homogeneous fault and short-range stress transfer. However, inhomogeneity plays an important role in the spatial and temporal behavior of an earthquake fault [10]. While a number of OFC models with nearest-neighbor stress transfer have been expanded to include inhomogeneity, generally by varying individual parameters along the fault plane [11-17], there have been no investigations of the effect of large-scale inhomogeneities in long-range models.

Stress transfer in natural earthquake faults is elastic and, as a result, OFC models with long-range stress transfer produce more realistic representations [18,19]. Moreover, it has been shown in several studies that the physics of long-range models is significantly different from that of short-range stress transfer models (see Supplementary Material). For example, OFC models with short-range stress transfer are not in equilibrium, while for infinite-range stress transfer the model is in equilibrium [19,20]. In addition, if the stress transfer range becomes large enough, it is reasonable to approximate the model by a mean-field theory [19].

A long standing problem in understanding the statistical distribution of earthquakes is how to reconcile GR scaling, which suggests the presence of a critical point, with the existence of foreshocks, aftershocks and quasi-periodic large events. Proposed mechanisms for understanding GR scaling, including self-organized critical phenomena (SOC) and cascade mechanisms, do not generate the clustering of foreshocks and aftershocks in conjunction with quasi-periodic large events. The approach presented here is to modify a model that explains GR scaling [19] by adding structural asperities which leave that scaling intact but produce clustering of foreshocks and aftershocks as well as large, regularly recurring events (detailed discussion of modified GR scaling is included in the Supplementary Material).

Inhomogeneities in the form of stress-relieving micro-cracks have been incorporated into long-range OFC [10,19] models, resulting in a better understanding of GR scaling [21]. In addition, inhomogeneities have been introduced into fully elastic models resulting in either power-law statistics of event sizes or a separate distribution combined with large, system size events [22]. However, to date, none of these approaches has reproduced both the temporal clustering and the complete magnitude-frequency distribution scaling regime that are primary features of natural seismicity and a critical component in the assessment of earthquake hazard.

Motivated by the structure of natural faults, we introduce heterogeneity in the form of asperities into the OFC model with long-range stress transfer. The introduction of these spatial heterogeneities produces temporal clustering similar to that seen in natural faults, including aftershocks, foreshocks and large events with constant return period.

Spatial and temporal clustering has long been recognized in seismicity data, and significant efforts have focused on those that occur in the same general region as the mainshock and immediately before (foreshocks) or immediately after (aftershocks) its occurrence [23-28]. Aftershocks occur close to their triggering mainshocks and the aftershock rate generally decays with time, following the power law relation known as the modified Omori law [25,27]. On the other hand, while precursory seismic activity, or foreshocks, have been recorded before a number of large events, their signal is much more difficult to observe [29-33].

One particular foreshock pattern, accelerating moment release (AMR) [30,32,34-37] is defined by the equation $\varepsilon(t)=A+B(t_f-t)^m$. $\varepsilon(t)$ has been interpreted as either the accumulated seismic moment or Benioff strain release within a specified region, from some origin time t_0 to time t. A is a constant that depends on the background level of activity, t_f is the time of the mainshock, B is negative and m is between 0.3 and 0.7. Ben-Zion et al. [38] analyzed the deformation preceding large earthquakes and obtained a 1-D power-law time-to-failure AMR relationship before large events when the seismicity had broad frequency-size statistics, consistent with observed seismic activation before some large earthquakes [39,40].

The ETAS (Epidemic Type Aftershock Sequences) model [41,42] is a triggering model used to simulate natural foreshock and aftershock sequences. It is based on the concept that every event, regardless of its size, increases the probability of later events. In ETAS, mainshocks trigger aftershocks, including those with magnitudes larger than themselves. If the largest event is triggered by smaller events, these are classified as foreshocks. While ETAS can replicate many clustering features seen in natural seismicity, recent work suggests that these triggering models may not fully explain the foreshock-mainshock-aftershock process and that other mechanisms may be important [32,43,44]. For example, Chen and Shearer [45] studied foreshock sequences for M>7 earthquakes in California and determined that they behaved more like swarms initiated by aseismic transients rather than triggered cascades or a nucleation process. These sequences occurred in areas of significant fault zone complexity, highlighting the importance of heterogeneity in the clustering process.

Our model is a two-dimensional cellular automaton with periodic boundary conditions based on the OFC [8] and RJB [3,7] models that incorporates heterogeneity into the lattice. Every site can redistribute released stress to all z neighbors within a radius, or stress interaction range, R. A homogeneous residual stress σ^r is assigned to all the sites in the lattice. To impose spatial inhomogeneity on the lattice, two sets of failure thresholds are introduced; 'regular sites' with a failure threshold of σ^f and 'asperity sites' with a significantly higher failure threshold ($\sigma^f_{(asperity)}=\sigma^f+\Delta\sigma^f$).

Initially, an internal stress variable, $\sigma_j(t)$, is randomly distributed to each site; the stress on every site falls between the residual stress and failure stress thresholds ($\sigma^r<\sigma_i(t=0)<\sigma^f$). At t=0 no sites will have $\sigma_i > \sigma^f$. We use the so-called zero velocity limit [8,46,47] to simulate the increase in stress associated with the dynamics of plate tectonics. The lattice is searched for the site that is closest to failure; i.e., the site with minimum (σ^f-σ_i). Then, this amount of stress, (σ^f-σ_i), is added to each site such that the stress on at least one site is equal to its failure threshold. The site fails and some fraction of its stress, given by $\alpha[\sigma^f-(\sigma^r \pm \eta)]$, is dissipated from the system. α is the dissipation parameter ($0<\alpha\leq 1$) which quantifies the portion of stress dissipated from the failed site and η is randomly distributed noise. Stress on the failed site is lowered to ($\sigma^r \pm \eta$) and the remaining stress is distributed to its predefined z neighbors. After the first site failure, all neighbors are searched to determine if the added stress caused additional failures. If so, the procedure is repeated. If not, the time step, known as the plate update (*pu*), increases by unity and the lattice is searched again for the site closest to failure (i.e., with the smallest (σ^f-σ_i)). The size of each event is calculated from the total number of failures resulting from the initial failure. Stress is dissipated from the system both at regular lattice sites and through asperity sites placed randomly throughout the system. However, asperity sites fail less frequently than the regular sites, providing a time-dependent source and sink of stress: storing dissipated stress until an asperity failure releases it back into the system. Addition of these large failure threshold heterogeneities, or localized stress accumulators, results in a rich pattern of temporal clustering that includes the occurrence of large events with constant return period (here designated ‘characteristic events’), foreshocks and aftershocks.

Here we investigate a system with 1% of randomly distributed asperity sites in a two-dimensional lattice of linear size L=256, R=16, and periodic boundary conditions. Every failed site directly transfers stress to z=1088 neighbors. The homogeneous failure threshold for the regular sites is σ^f=2.0, homogeneous residual stress for the entire lattice is σ^r=1.0, with random uniform noise distribution of η=[-0.1,+0.1]. The failure threshold for asperity sites is designated $\sigma^f_{(asperity)}=\sigma^f+10$.

We compare our inhomogeneous model and a homogeneous model with no asperity sites in Fig.1. Time series of 6*10^5 p.u. and frequency distributions of 10^7 p.u are shown for three different values of stress dissipation parameter α. The first diagram (*i*) in each set is the time series for the heterogeneous model with 1% of asperity sites. Time steps in which an asperity site breaks are highlighted with a grey background shade. The second diagram (*ii*) is the time series for the homogeneous model (no asperity sites). Comparison between the frequency distribution for different values of α, with and without asperities, is shown in Fig1.d. For the 1% asperity model the lattice does not break randomly in time, despite the random spatial distribution of asperities. The asperity model produces large, repeating events that recur at constant intervals. *Those characteristic events occur less frequently as α, the stress dissipation, increases*. The distributions also confirm that, *as α increases, the largest events become smaller,* because higher stress dissipation suppresses large events [19]. The 1% asperity model generates larger events compared to the homogeneous model.

In Fig.2, we isolate a single activation sequence for α=0.2 and α=0.4 (Fig.2a and 2b, respectively). Temporal clustering is clearly visible (Fig.2a and 2b, *i* and *ii*), starting with a gradually increasing number of larger events (foreshocks) and ending with a tail of decreasing activity (aftershocks). Results for α=0.6 (not shown) are qualitatively similar. The temporal clustering is primarily a result of the asperities. Increased α again reduces the size of the largest events (Fig.2a and 2b, *iii*). In addition, the increasing number of events prior to the mainshock is analogous to the increased rate of activity, or AMR, observed before some large earthquakes (Fig.2a and 2b, *iv*). Because changes in the bin length strongly affect the slope in Figs.2(a-*iv*) and 2(b-*iv*), additional study is needed for proper comparison with naturally occurring earthquake sequences; however, increased stress dissipation appears to increase the steepness of the AMR curve (Fig.2a and 2b, *iv*). This is the first time this complete set of phenomena has been observed in the OFC/RJB class of models.

While most theoretical models of earthquake seismicity such as ETAS presuppose that all events are governed by the same physics, recent careful analysis has suggested that variation in foreshock-aftershock rates may be dependent on the local or regional rheology. Enescu et al. [44] demonstrated that swarm-type seismic activity with higher foreshock rates occurred in areas of California with relatively high surface heat flow, while more typical sequences occurred in regions with lower heat flow. McGuire et al. [48] analyzed hydroacoustic data along East Pacific Rise faults and identified sequences with higher foreshock rates and lower aftershock rates than previously observed in continental transform faults, or a relatively high ratio of foreshocks to aftershocks.

We performed a similar analysis for a swarm in the southern Eyjafjarðaráll graben off the north coast of Iceland, late summer of 2012 (Fig.3a). Of the fifteen largest events ($M \geq 2.5$), eight were associated with foreshock and/or aftershock clusters that could be distinguished from the background activity. The spatiotemporal distribution of those foreshock and aftershock events, relative to their respective mainshocks, is plotted in Fig.3b, while the GR relationship and AMR plot are shown in Fig.3c and 3d, respectively. The similarity to Fig.2 provides evidence for natural cases in which foreshock abundance is of the same order of magnitude and duration as aftershock sequences. Although the spatial clustering seen in Fig.3b is not reproduced in the model (Fig.2*ii*), ongoing work suggests that this is a result of the random spatial distribution of asperities.

In order to better understand how the relative production of foreshocks and aftershocks is governed by the model parameters, we investigated the length of the average foreshock and aftershock periods for different values of α in our model. In general, lower dissipation favors more frequent, larger events and higher dissipation suppresses the large events (Fig.1.d). Stress dissipation also appears to have an effect on the relative length of those foreshock sequences. In Fig.4 we plot the relative length of the foreshock and aftershock sequences, normalized by the total time period of each sequence. For low α values, the energy, or stress, available for foreshock activity is greater and initially results in an increased number of foreshocks, breaking more asperities. Once the mainshock occurs, there are fewer unbroken sites available for the occurrence of aftershocks. As a result, the aftershock sequence is shorter. On the other hand, in higher dissipation systems, it is not until the occurrence of the largest event, the mainshock, that enough stress is injected into the surrounding sites to initiate failure of large numbers of additional sites as aftershocks. High dissipation results in shorter foreshock sequences and relatively longer aftershock sequences (Fig.4). The average number of events is lower in models with higher α, but the length of the total activity period also appears to be related to α. Because higher values of alpha suppress large events, more plate updates are required to fail all the asperities in higher dissipation models..

In summary, we present a long-range OFC model with randomly distributed asperities. While the asperities do not change the GR relation proposed in [19], this heterogeneity introduces temporal clustering similar to that seen in natural fault systems. Unlike previous versions of the OFC model, we observe “quasi-periodic” characteristic earthquake sequences associated with periods of activity which start with gradually increasing numbers of larger events, or foreshocks, and end with a tail of decreasing activity, or aftershocks (Fig.2). The relative length of the foreshock and aftershock sequences varies, as observed in different tectonic regions (Fig.3). The length of the foreshock and aftershock activation is related to one or more controlling parameters of the model, including the stress dissipation (Fig.4), providing a potential explanation for the observation that certain tectonic regimes, such as mid-ocean ridges, have measurable foreshock sequences, while others, such as crustal transform faults, produce few foreshocks.

The results from this simple model suggest that asperities are partly responsible for the time-dependent behavior observed in natural earthquake fault systems. In the model, asperities act as stress reservoirs that remove and store stress until their failure threshold is reached. Once that threshold is reached, the asperity failure releases a large amount of stress into the system over a short time. This often results in a very large event. Between asperity failures the model behaves as if it is an OFC model without asperities but with large dissipation, since the stress is removed and stored in the asperities, resulting in attenuated GR scaling and large, quasi-periodic events. The smaller stochastic, GR scaling events which result from the triggering process have a small impact on the event statistics due to the large separation of failure thresholds. This interplay of triggering and structure provides new insights into the variation in the statistical event distributions from one model, or fault, to another. That variation is governed by the distribution and strength of the asperities.

The implication of our results is that the spatial and temporal patterns observed in natural seismicity are controlled by the fault structure as well as a triggering process. A fault with strong asperities will produce large quasi-periodic events combined with a small GR scaling region. If there are no asperities then the dominant process will be triggering and the fault will produce a large GR scaling regime. This interpretation allows for a smooth transition between those two modes, as is seen in many natural fault systems. This hypothesis can be tested. We should be able to differentiate between faults with strong asperities and those with weaker or fewer weaker asperities, based upon their magnitude-frequency distribution.

This work also demonstrates that it is possible to link the underlying physical properties to measurable parameters of the spatial and temporal patterns observed in natural seismicity, such as Omori exponent, stress drop or inter-event time. If spatial heterogeneity affects the spatiotemporal behavior of earthquake sequences, including earthquake return period and precursory activity (foreshocks), then it should be possible to link stress dissipation and asperity distribution to the foreshock-aftershock duration and inter-event times, potentially allowing us to improve their predictability. The fact that the precursory patterns in earthquake fault networks are controlled by these spatial heterogeneities provides a new paradigm with which to investigate and quantify the relationship between fault structure, spatiotemporal clustering, and earthquake predictability.

Acknowledgements

This research was funded by the NSERC and Aon Benfield/ICLR IRC in Earthquake Hazard Assessment, and an NSERC Discovery Grant (JK and KFT). WK was funded by a grant from the DOE.

We also would like to thank the Icelandic Met Office for providing seismic data on the 2012-2013 Eyjafjarðaráll swarm. GMT software [49] was used to create the figures.

[1] R. Burridge and L. Knopoff, Model and theoretical seismicity, Bull. Seismol. Soc. Am. 57. 341–371, (1967).

[2] M. Otsuka, A Simulation of earthquake occurrence, Phys Earth Planet Inter. 6-311, 1972.

[3] J. B. Rundle and D. D. Jackson, Numerical simulation of earthquake sequences, Bull. Seismol. Soc. Am. 67, (1977).

[4] J. B. Rundle, A physical model for earthquakes, J. Geophys. Res. 93-6237, 1988.

[5] J. M. Carlson, and J. S. Langer, Mechanical model of an earthquake fault. Phys. Rev. Lett. 62, 2632; Phys. Rev. A 40, 6470, (1989).

[6] H. Nakanishi, Cellular-automaton model of earthquakes with deterministic dynamics. Phys. Rev. A 41, 7086, (1990).

[7] J. B. Rundle and S. R. Brown, Origin of Rate Dependence in Frictional Sliding, J. Stat. Phys. 65, 403, (1991).

[8] Z. Olami, HJS. Feder, K. Christensen, Self-organized criticality in a continuous, nonconservative cellular automaton modeling earthquakes. Phys Rev Lett 68(8):1244–1247, (1992).

[9] M. J. Alava, P. Nukala, and S. Zapperi, Statistical models of fracture, Adv. Phys. 55, 349, (2006).

[10] R. Dominguez, K.F. Tiampo, C.A. Serino and W. Klein, Scaling of earthquake models with inhomogeneous stress dissipation. Phys. Rev. E 87, 022809, (2013).

[11] I.M. Janosi and J. Kertesz, Self-organized criticality with and without conservation. Physica A, 200, 0378, (1993).

[12] F. Torvund and J. Froyland, Strong ordering by non-uniformity of thresholds in a coupled map lattice. Physica Scripta 52, 624, (1995).

[13] H. Ceva, Inhuence of defects in a coupled map lattice modelling earthquakes. Phys. Rev, E52, 154, (1995).

[14] N. Mousseau, Synchronization by Disorder in Coupled Systems. Phys. Rev. Lett. 77, 968, (1996).

[15] O. Ramos, E. Altshuler and K.J. Maloy, Quasiperiodic Events in an Earthquake Model. Phys. Rev. Lett. 96, 098501, (2006).

[16] M. Bach, F. Wissel and B. Dressel, Olami-Feder-Christensen model with quenched disorder. Phys. Rev. E 77, 067101, (2008).

[17] E.A. Jagla, Realistic spatial and temporal earthquake distributions in a modified Olami-Feder-Christensen model. Phys. Rev E 81, 046117, (2010).

[18] Y. Ben-Zion, Collective Behavior of Earthquakes and Faults: Continuum-Discrete Transitions, Progressive Evolutionary Changes and Different Dynamic Regimes, Rev. Geophysics, 46, RG4006, doi:10.1029/2008RG000260, (2008).

[19] C.A. Serino, K. F. Tiampo, and W. Klein, New Approach to Gutenberg-Richter Scaling, Phys. Rev. Lett. 106, 108501, (2011).

[20] W. Klein, H. Gould, N. Gulbahce, J. B. Rundle and K. F. Tiampo, Structure of fluctuations near mean-field critical points and spinodals and its implication for physical processes. Phys. Rev. E 75, 031114 (2007)"

[21] C. F. Richter, An instrumental earthquake magnitude scale. Bull. Seismol. Soc. Am. 25, 1-32, (1935).

[22] D. S. Fisher, K. Dahmen, S. Ramanathan and Y. Ben-Zion, Statistics of earthquakes in Simple Models of Heterogeneous Faults, Phys. Rev. Lett., 78, 4885-4888 (1997).

[23] M. Båth, Lateral inhomogeneities of the upper mantle, Tectonophysics, 2, 483–514, (1965).

[24] H. Kanamori, The nature of seismicity patterns before large earthquakes, in Earthquake Prediction, Maurice Ewing Series, IV, 1–19, AGU, Washington D.C., (1981).

[25] Y. Ogata, Estimation of the Parameters in the Modified Omori Formula for Aftershock Frequencies by the Maximum Likelihood Procedure. Journal of Physics of the Earth 31, 115–124, (1983).

[26] T. Utsu, Y. Ogata and R.S. Matsu'ura, The centenary of the Omori formula for a decay law of aftershock activity. Journal of Physics of the Earth 43, 1–33, (1995).

[27] D.A. Dodge, G.C. Beroza and W.L. Ellsworth, Detailed observations of California foreshock sequences: Implications for the earthquake initiation process. J. Geophys. Res., 101 (B10), pp. 22371–22392, (1996).

[28] R. Shcherbakov and D. L. Turcotte, A modified form of Båth's law, Bull. Seismol. Soc. Am., 94, 1968–1975, (2004).

[29] W.H. Bakun, B. Aagaard, B. Dost, W.L. Ellsworth, J.L. Hardebeck, R.A. Harris, C. Ji, M.J.S. Johnston, J. Langbein, J.J. Lienkaemper, A.J. Michael, J.R. Murray, R.M. Nadeau, P.A. Reasenberg, M.S. Reichle, E.A. Roeloffs, A. Shakal, R.W. Simpson and F. Waldhauser, Implications for prediction and hazard assessment from the 2004 Parkfield earthquake. Nature 437, 969–974, (2005).

[30] W.L. Ellsworth, A.G. Lindh, W.H. Prescott and D.J. Herd, The 1906 San Francisco earthquake and the seismic cycle, in Earthquake Prediction: An Internation Review, Maurice Ewing Ser. Edited by D.W. Simpson and P. G. Richards. 4: 126-140, (1981).

[31] T.H. Jordan and L.M. Jones, Operational earthquake forecasting: some thoughts on why and how. Seismological Research Letters 81, (2010).

[32] L.R. Sykes and S.C. Jaumé, Seismic activity on neighbouring faults as a long term precursor to large earthquakes in the San Francisco Bay area. Nature. 348: 595-599, (1990).

[33] P. M. Shearer, Self-similar earthquake triggering, Båth's law, and foreshock/aftershock magnitudes: Simulations, theory, and results for southern California, J. Geophys. Res., 117, B06310, (2012).

[34] D. D. Bowman and G. C. King, Accelerating seismicity and stress accumulation before large earthquakes. Geophys. Res. Letters. 28: 4039-4042, (2001).

[35] D. D. Bowman, G. Ouillon, C. G. Sammis, A. Sornette and D. Sornette, An observational test of the critical earthquake concept. J. Geophys. Res.103 (B10): 24,359 24,372, (1998).

[36] D. Sornette and C. G. Sammis, Complex critical exponents from renormalization group theory of earthquakes: Implications for earthquake predictions, J.Phys.I France 5, 607-619, (1995).

[37] C. G. Bufe and D. J. Varnes, Predictive modeling of the seismic cycle for the greater San Francisco Bay region. J. Geophys. Res. 98: 9871-9883, (1993).

[38] Y. Ben-Zion and V. Lyakhovsky, Accelerating seismic release and related aspects of seismicity patterns on earthquake faults, Pure Appl. Geophys., 159, 2385–2412, (2002).

[39] D. L. Turcotte, W. I. Newman and R. Shcherbakov, Micro and macroscopic models of rock fracture. Geophys. J. Int., 152, 718–728, (2003).

[40] G. Zoller, S. Hainzl, Y. Ben-Zion and M. Holschneider, Earthquake activity related to seismic cycles in a model for a heterogeneous strike-slip fault, Tectonophys., 423, 137–145, (2006).

[41] Y. Ogata, Seismicity analysis through point-process modeling: A review, Pure Appl. Geophys., 155, 471–507, (1999).

[42] A. Helmstetter and D. Sornette, Diffusion of epicenters of earthquake aftershocks, Omori's law, and generalized continuous-time random walk models, Phys. Rev. E., 66, 061104, (2002).

[43] D.A. Dodge and G. C. Beroza, Source array analysis of coda waves near the 1989 Loma Prieta, California, mainshock: Implications for the mechanism of coseismic velocity changes. J. Geophys. Res. 102, 24437−24458, (1997).

[44] B. Enescu, S. Hainzl and Y. Ben-Zion, Correlations of seismicity patterns in southern California with surface heat flow data. BSSA, 99(6): 3114-3123, (2009).

[45] X. Chen and P. M. Shearer, California foreshock sequences suggest aseismic triggering process, doi: 10.1002/grl.50444 (2013).

[46] J. M. Carlson, J. S. Langer, B. E. Shaw, and C. Tang, Phys. Intrinsic properties of a Burridge-Knopoff model of an earthquake fault Rev. A 44, 884 (1991).

[47] J. Xia, H. Gould, W. Klein, and J.B. Rundle. "Near-mean-field behavior in the generalized Burridge-Knopoff earthquake model with variable-range stress transfer". Phys. Rev. E 77 , 031132, (2008).

[48] J. J. McGuire, M. S. Boettcher and T. H. Jordan, Foreshock sequences and short-term earthquake predictability on East Pacific Rise transform faults, Nature, 434, (2005).

[49] P. Wessel and W. H. F. Smith, New, improved version of Generic Mapping Tools released. EOS Trans. Am. Geophys.Union 79, 579, (1998).

[50] See Supplementary Material [url] which includes Refs. [51-64]

[51] M. Kac, G. E. Uhlenbeck, and P. Hemmer, On the van der Waals Theory of the Vapor-Liquid Equilibrium. I. Discussion of a One-Dimensional Model, J. Math. Phys. 4, 216 (1963).

[52] J.L. Lebowitz and O. Penrose, Rigorous Treatment of the van der Waals-Maxwell Theory of the Liquid-Vapor Transition, J. Math. Phys. 7, 98 (1966).

[53] Tsallis, C. (2001). Nonextensive Statistical Mechanics and Thermodynamics: Historical Background and Present Status. In Nonextensive statistical mechanics and its applications / Sumiyoshi Abe;YukoOkamoto(ed.): Springer,(Lecture notes in physics ; Vol. 560) (Physics and astronomy online library) ISBN 3-540-41208.

[54] N. Gulbahce, H. Gould, and W. Klein, Zeros of the partition function and pseudospinodal in long-range Ising models, Phys. Rev. E 69, 036119 (2004).

[55] W. Klein, M. Anghel, C.D. Ferguson, J.B. Rundle, and Sá Martins J.S., in Geocomplexity and the Physics of Earthquakes, ed. by Rundle, J.B., Turcotte, D.L. and Klein, W., Geophysical Monograph Vol. 120 (AGU, Washington D.C.) p. 43 (2000).

[56] J.B. Rundle, W. Klein, S. Gross, and D.L. Turcotte, Boltzmann Fluctuations in Numerical Simulations of Nonequilibrium Lattice Threshold Systems, Phys. Rev. Lett. 75, 1658 (1995).

[57] J.B., Rundle, W. Klein, K. Tiampo, and S. Gross, Linear Pattern dynamics in nonlinear threshold systems, Phys. Rev. E, 61 (3), 2418–2431 (2000).

[58] R. Dominguez, K. Tiampo, C.A. Serino and W. Klein, Geophysical Monograph Series. 196, 41-54. doi:10.1029/2011GM001082 (2012).

[59] B. Gutenberg and C.F. Richter, Magnitude and energy of earthquakes, Annali di Geofisica, Vol. 9, n. 1 (1956).

[60] D.L. Turcotte, D. L. Fractals and chaos in geology and geophysics, 2nd edn. Cambridge, UK: Cambridge University Press (1997).

[61] I. Main, Statistical physics, seismogenesis, and seismic hazard, Rev. Geophys. 34, 433–462 (1996).

[62] Y.Y. Kagan and D.D. Jackson, Probabilistic forcasting of earthquakes, Geophys. J. Int., 143, 438-453 (2000).

[63] A.F. Bell, M. Naylor, I.G. Main, Convergence of the frequency-size distribution of global earthquakes, GRL, 40, 2585–2589, doi:10.1002/grl.50416 (2013).

[64] G. Zoller, M. Holschneider, S. Hainzl, The Maximum Earthquake Magnitude in a Time Horizon: Theory and Case Strudies, BSSA 2013; 103 (2A) : 860-875 (2013).

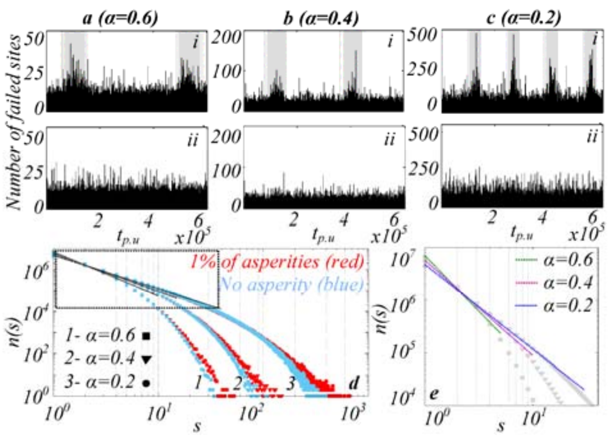

Fig.1. Time series of events (number of failed sites) over $6*10^5$ plate updates for: (a) α=0.6, (b) α=0.4 and (c) α=0.2; (*i*) 1% of randomly distributed asperity sites (shaded background are times when an asperity site breaks); (*ii*) homogeneous model with the same conditions as (i). (d) Comparison between frequency distributions n(s), with and without 1% of randomly distributed asperity sites, for three values of α. Slope of the linear fit to *a-iii*=2.00, *b-iii*=1.85, and *c-iii*=1.65. (e) Close-up of the box in (d).

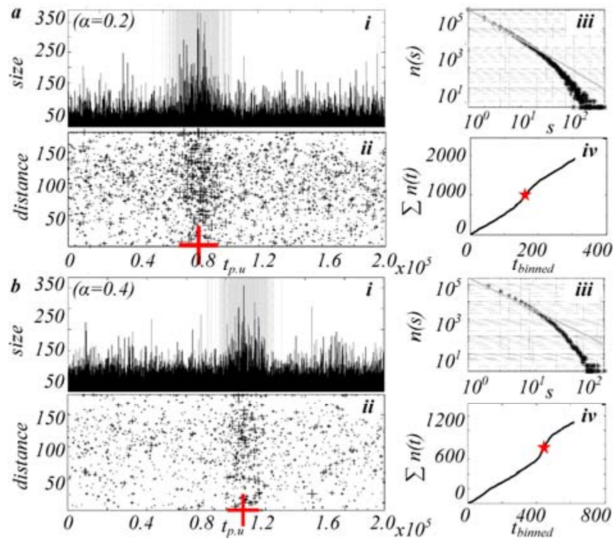

Fig.2. (a-*i*) Number of failed sites at each time step (shaded background as in Fig.1) for α=0.2. Time is binned into coarse-grained units of Δt=500pu. (a-*ii*) Distance of each event from the largest event in the sequence (mainshock, red cross). (a-*iii*) Distribution of events, n(s), during the period (a-*i*). Slope for the straight line fit is 1.6 (a-i*v*) Cumulative number of events greater than the defined threshold versus coarse-grained time. (b-*i*, *ii*, *iii*, *iv*) as in (a) for stress dissipation of 40% (α=0.4). Slope of the linear fit to *b-iii* is 1.85.

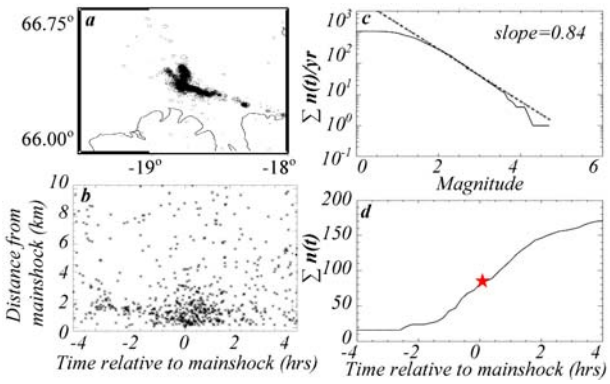

Fig.3. (a) Seismicity for swarm event, southern Eyjafjarðaráll graben, Aug 20, 2012 through March 25, 2013. Most activity occurred between the graben and the Húsavík-Flatey fault. (b) Spatiotemporal distribution of seismicity associated with the twelve largest events in the sequence in (a). Note that earthquake magnitude is logarithmic, where every unit increase is equivalent to approximately 32 times the energy increase. (c) GR distribution for the longest single sequence in the swarm, $M \geq M_c = 2.0$, M_c is minimum magnitude of completeness. (d) Cumulative number of events greater than M_c versus time relative to the mainshock (star, M=4.76). Data collected by the SIL network was provided by the Icelandic Met Office (en.vedur.is).

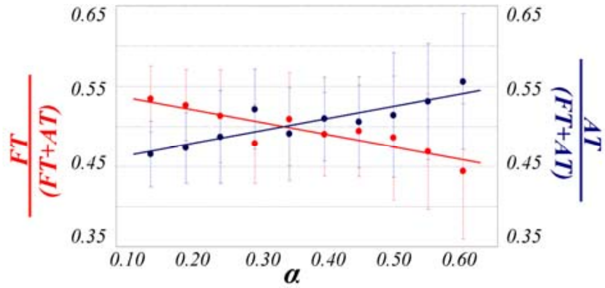

Fig.4. The average time period associated with foreshocks and aftershocks as a function of *α*, 1% of randomly distributed asperity sites. FT=Foreshock time; AT=Aftershock time; Red=FT/(FT+AT); Blue=AT/(FT+AT); (FT+AT)=total sequence.